Reflectivity Reduction of Retro-Reflector Installed in LHD due to Plasma Surface Interaction

N. Yoshida[1)], Y. Ohtawa[2)], A. Ebihara[2)], T.Akiyama[3)], M. Tokitani[3)], N. Ashikawa[3)], K. Kawahata[3)]

[1)] Research Institute for Applied Mechanics, Kyushu University, Kasuga, Fukuoka, 816-8580, Japan

[2)] Graduate School of Engineering Sciences, Kyushu University, Kasuga, Fukuoka, 816-8580, Japan

[3)] National Institute for Fusion Science, Oroshi, Toki, Gifu 509-5292, Japan

E-mail: yoshida@riam.kyushu-u.ac.jp

Abstract : Optical reflectivity of the retro-reflector installed in LHD as the first mirror was reduced seriously by plasma wall interaction. In order to understand the mechanism of the reflectivity reduction, optical and material properties of the mirror surfaces have been examined extensively. It was found that the deposited impurity layers caused the serious reduction of the reflectivity. Formation of iron oxide, bulges structure and He bubbles are the major factors for the reflectivity reduction in the wide wave length range.

1. Introduction

Plasma facing surfaces of in-vessel components in fusion devices suffer very strong plasma wall interactions (PWI) and their surface properties change due to irradiation damage by energetic plasma particles and by re-deposition of impurities. This phenomenon is well recognized as serious issue for first walls and divertors. On the other hand, so called first reflectors for plasma diagnostics utilizing laser are placed on the first wall or in the ports near the first wall. Degradation of their optical properties due to PWI is also great concern. Suppression of reflectivity degradation is very important to keep high reliability of the diagnostics. Though the optical reflectors in the present plasma devices can be replaced whenever the reflectivity dropped, it will be difficult to change them often in the D-T burning devices such as ITER. Development of optical reflectors with longer life time is argent issues.

Reduction of optical reflectivity due to the interaction with plasma has been studied from various viewpoints such as material dependence [1-6]. It is not easy to evaluate the reduction of reflectivity for each reflector in ITER, because the phenomena also depend strongly on the characteristics of plasma surrounding it [7-8]. In large high temperature plasma confinement devices operating at present many first reflectors are used in various different plasma environments. It will be very useful to analyze the mechanism of reduction for these reflectors.

In case of the large helical device (LHD), three retro-reflectors were fixed on the first wall in the 3rd and 4th campaigns for electron density measurement with CO_2 laser [9]. In the preset work, reflectivity for wide range of optical wave length, surface morphology, surface chemical composition and internal structure at subsurface regions of the reflectors were measured to under stand the plasma-wall interaction causing the degradation of the optical reflectivity.

2. Experimental Procedures

2.1 Retro-reflectors used in LHD

Corner cube reflectors called as retro-reflectors are composed of three flat mirrors meeting at right angles each other. The inner cubic corner, where the three mirrors meet, is used as a reflector, because the reflected ray is always parallel to the incident one independently on the incident angle. This type reflector is often used, because it makes easier the optical alignment of plasma diagnostic system. As shown in Fig. 1 (a), the retro-reflectors used in the cycle 4 were protected by a cylinder made of 303SS. Each mirror made of 316SS was plated with gold of about 300nm-thick to get high optical reflectivity [9]. The positions of the retro-reflectors in the LHD are illustrated in Fig. 1(b). The main plasma can be widely viewed from the position. In the present work, the retro-reflector of the Ch 1, which is closest to the plasma, was examined mainly. The reflectors were exposed not only to the main plasma discharges of hydrogen and helium but also helium plasma of about 200eV for glow discharge cleaning (GDC) through the whole experimental cycle.

It was reported that the optical reflectivity for CO_2 laser decreased during rather long glow discharge cleaning for the start-up of the cycle and following main plasma discharges and glow discharge cleaning [9]. The materials of the inner wall of vacuum vessel (protection wall) and the divertor were 304 SS, whose main components were Fe, Ni and Cr, and isotropic graphite, respectively.

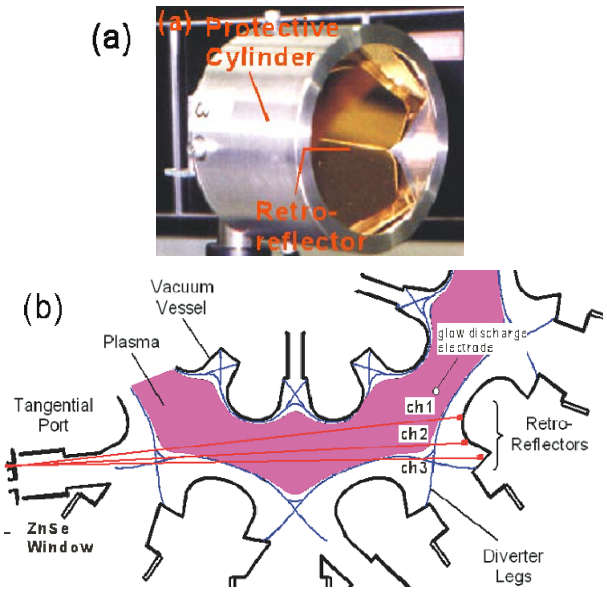

Fig. 1 (a) Retro-reflectors installed in LHD. Gold-plated flat reflectors are seen. (b) Positions of the retro-reflectors and laser beams are shown.

2.2 Measurements of optical reflectivity

Optical reflectivity at the mirror surface was measured by ultraviolet-visible-near infrared spectrophotometer for wave length between 190nm and 2500nm and Fourier transform

infrared spectrophotometer (FTIR) for 1500nm~25000nm. The diameter of the laser beam for the measurement was 3mmϕ for the both instruments and incident angle was less 3 º and 5º, almost perpendicular to the mirror surface.

2.3 Observation of surface morphology and internal structure

Scanning electron microscope (SEM) with energy dispersive X-ray spectrometer (EDS) was used for observation of surface morphology and chemical element analysis. The height of surface roughness was measured by stereoscopic observation technique. In order to examine microstructure of the subsurface region by TEM and STEM with EDS, cross-sectional micro samples were made by using focused iron beam technique (FIB).

3. Experimental Results

3.1 Optical reflectivity

Photographs of the retro-reflector and its three flat mirrors are shown in Fig.2. As can be seen, strong blacking, namely reduction of optical reflectivity, occurred especially at the cubic corner where three mirrors contacted each other (corner at right-hand side in the photographs). Inspections were carried out mainly for the #1 mirror.

Figs. 3 and 4 show optical reflectivity measured at the five points **a, b**, **c**, **d** and **e** from the aperture edge to the cubic corner of the reflector as denoted on the photo in Fig. 2 (b). Discrete data at 900nm in Fig.3 was caused by changing the detectors at this wave length. Reflectivity of a stainless steel mirror and a gold mirror are also plotted in the figure for comparison. The area near the aperture edge had lost the original gold color but shows a typical gloss of metals. As can be seen in Fig. 3, reflectivity spectrum at the point **a** is quite similar to that of stainless steel. Point **b** corresponds to the narrow arc region having brown color. In contrast, the reflectivity at the points **c**, **d** and **e** decrease drastically by approaching to the cubic corner where the laser beam reflected. The reflectivity for short wave length below visible region is almost 0%. It is worth to note that the reduction of reflectivity at infrared region is also remarkable; for example, reflectivity reduction for CO_2 laser (wave length=10.6μm) at the points **d** and **e** is 50-60%. In case of retro-reflectors the substantial reflectivity is less than 20%, because reflection occurs three times.

3.2 Surface morphology and elemental components

In order to understand the reasons for the reflectivity degradation described in 3.1, observation of surface morphology and surface analysis were performed with SEM/EDS for the points from **a** to **e**. In Figs. 5 and 6 SEM micrographs and corresponding EDS spectrum for each point are summarized. On the surface of the point **a**, the coated gold layer has completely disappeared and the stainless steel substrate is bared. The surface has typical rough morphology of poly-crystals eroded by ion sputtering. On the other hand, the surface of the point **b** is very smooth and gold is a major component. This indicates that net erosion at the brown belt-like

region is almost zero and its surface has been kept original condition even after 4 months operation.

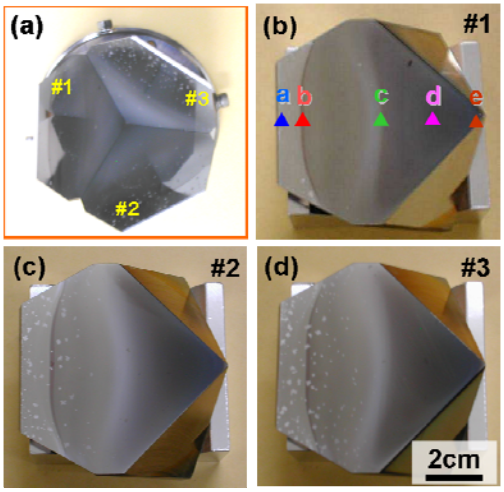

Fig.2 Photographs of a retro-reflector looking from the laser incident direction (a), and its three flat reflectors (b)-(d). Reflectivity and corresponding surface morphologies are mainly examined at the points ***a****,* ***b****,* ***c****,* ***d*** *and* ***e*** *of the #1 flat mirror.*

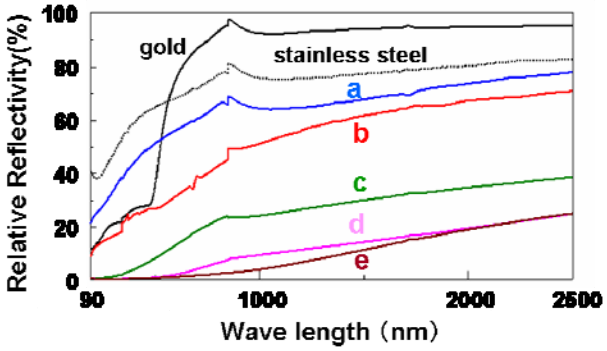

Fig.3 Reflectivity at the points ***a****,* ***b****,* ***c****,* ***d****, and* ***e*** *for the wave length between 90nm and 2500nm. Those for gold and stainless steel are also plotted in the figure.*

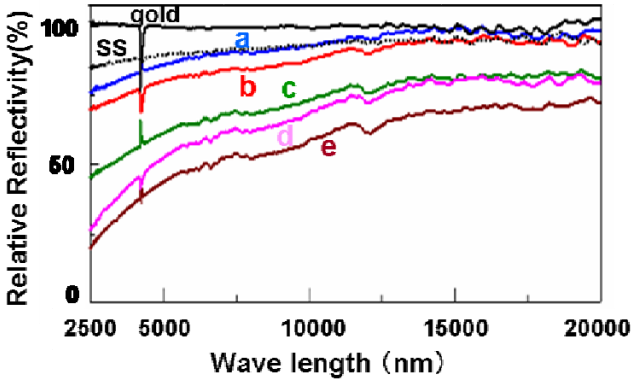

Fig. 4 Reflectivity at the points ***a****,* ***b****,* ***c,*** ***d****, and* ***e*** *for the wave length between 2500nm and 20000nm. Those for gold and stainless steel are also plotted.*

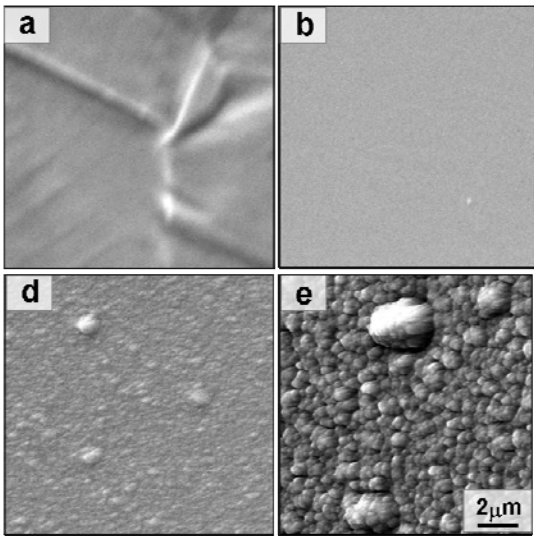

*Fig. 5 SEM micrographs showing surface morphology at points **a**, **b**, **d** and **e**.*

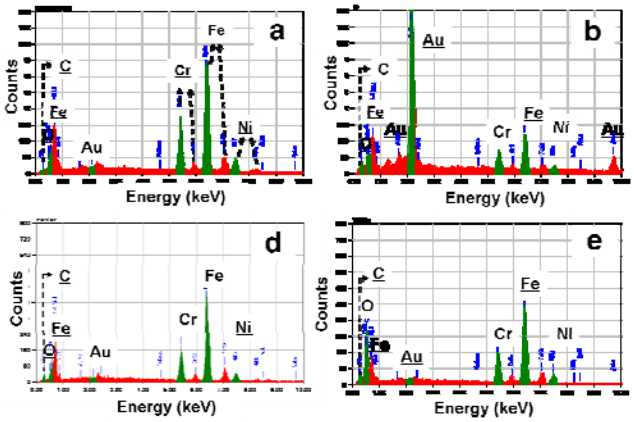

*Fig. 6 EDS spectrum showing chemical composition at the points **a**, **b**, **d** and **e**.*

Beyond the point **b** metallic gloss diminished gradually and the color of the surface turned to black. As shown in the SEM micrographs in Fig.5(d) and Fig.5(e), the surface is covered by fine sub-micron hills of about 200-800nm in diameter. In addition projections larger than 1μm in diameter exist in places. Height of the sub-micron hills and the large projections increases by approaching to the cubic corner.

Fig.7 is a magnified SEM micrograph showing details of the surface morphology. It is interesting that the sub-micron hills and the projections incline somewhat toward the left-hand side in the micrograph, namely toward the aperture of the retro-reflector. Development of the sub-micron hills in the left hand area of the large projection is delayed. The height of the sub-micron hills was estimated to be 100-500nm from the stereoscopic observation. Height of the large projection exceeds 2.5μm.

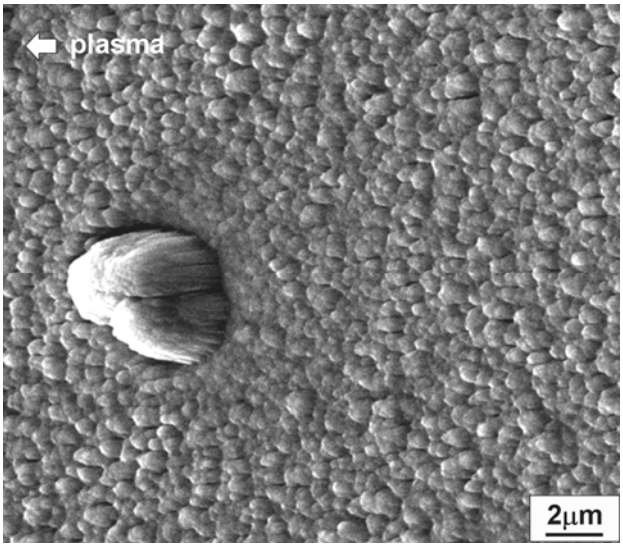

Fig. 7 Formation of sub-micron hills around a large projection, SEM micrographs at the point ***e****.*

EDS analysis shown in Fig.6 indicated that the major elements at the points **d** and **e** are Fe, Cr, Ni and O. Content of O is very large at the point **e**. These results indicate that majority of the deposited impurities came from the plasma. Fig. 8 is a SEM image where the deposition detached at the interface between the gold (point **e**). Thickness of the deposition is about 2μm.

In order to clarify the mechanism of reflectivity degradation, 180nm-thick nickel layer was deposited in vacuum on the surface of the mirror. This thickness is high enough to hide the optical properties of the original surface and change them to those of Ni, but thin enough to keep the surface morphology with sub-micron scale roughening. As can be seen in the photo of the mirror after Ni deposition in Fig.9,, influence of the original surface had gone and showed typical color of Ni in the area of the points **a** and **b** where the surface is rather smooth. In contrast, at the heavily blacken area (points **d** and **e**), the Ni deposition hardly changed the color. These results indicate that the major reason of the blacken near the cubic corner is the surface roughening by the formation of sub-micron-scale hills.

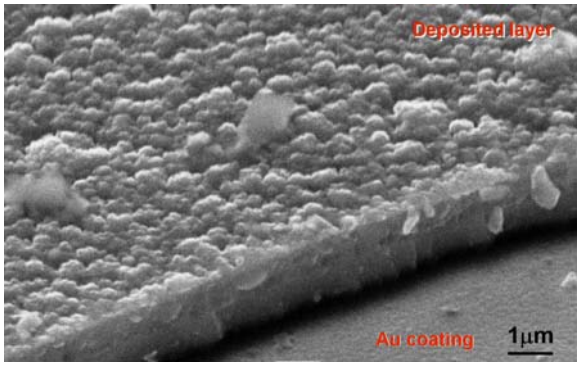

Fig. 8 SEM micrograph showing exfoliation of the deposited layer. Original Au-coated surface appeared after the exfoliation (lower right part).

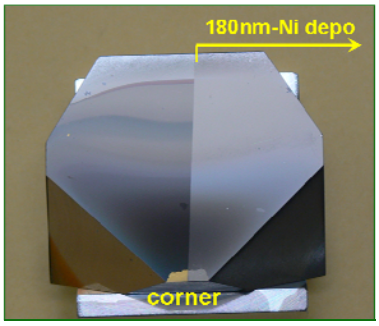

Fig. 9 Photograph of the reflector whose right-half was covered by a vacuum deposited Ni thin film of about 180nm thick.

3.3 Internal structure of the deposition

In order to understand the mechanism of the reflectivity reduction, cross-sectional structure and its chemical composition of the deposition were examined microscopically by using TEM and STEM with EDS. The thin cross sectional samples of about 200nm-thick were prepared by means of FIB technique from the area **e** shown in Fig. 2. Fig. 10 is cross-sectional TEM image of the deposition formed on the original mirror surface coated by MgF_2. It is remarkable that the deposition has clear layer structure. Up to about 0.67μm for the original mirror surface the layer was rather flat and has dark contrast. Above 0.67μm the layers become wavy suddenly and the wave inclines toward the main plasma direction just as expected from the SEM image shown in Fig. 7. The final thickness of the deposition is about 1.6μm in this case. The image of lower flat part is uniformly dark, while that of the upper wavy part is rather light. This result indicates that the average density of the former is high but that of the latter is low. EDS analysis indicates that Fe, Cr, Ni, Au and O are the major elements composing the deposition. Fig. 11 shows two dimensional distributions of deposited elements, O, Fe and Au together with the corresponding STEM image. The distribution of Cr and Ni are similar to that of Fe.

At the beginning of the experimental cycle long He glow discharge cleaning were performed previous to the main discharge experiments. As shown in Fig. 11, EDS data indicate that Au from the mirror itself, probably from the point **a** area shown in Fig. 2 where strong erosion occurred and the plated gold has gone, was deposited together with Fe and O form the protection wall made of stainless steel. Content of Au quickly decreased.

Characters of the deposition changed clearly at the hight of about 100nm. Above this level the content of O increased discontinuously and then gradually decreased up to 670nm by reaping fluctuation. A typical microstructure of this area (point A in the figure) is shown in Fig.12 (a). The deposition is composed of very fine crystals. The electron diffraction pattern (EDP) indicates that most of them are FeO crystals. It is remarkable that the nano-scale bubbles having white dot image were formed densely together with large bubbles of about 10-40nm in size. It is likely that high pressure gas of He and H exist in these bubbles.

The looking of the deposition drastically change above 670nm. Fig.12(b) is the magnified micrograph at the interface and EDP from the upper region. Just above the interface the

deposition is hollow (large white region in the micrograph). Content of O is very high and large FeO crystals of about 10-30nm in diameter are formed. The most prominent feature is the deposition is not flat but very complicate. The dotted lines in the figure trace the layer with dark image of about 100nm-thick. It is clear that the layers have half-circle shape of about 500-600nm in diameter extending from the interface. It is also important that below the half-circle dense layer, there is a large hole. Taking into account that the thickness of the sample is about 100nm, these images indicates that they are blisters with shape of half-sphere domes of about 300nm-high. They are densely formed at the interface. The material of the blisters is mainly fine FeO crystals and dense nano-scale bubbles are formed in it. After the formation of the blisters surface of the deposition becomes wavy and wavy with increasing the thickness of the deposition.

A magnified micrograph and EDP near the top surface (point C in Fig. 11) is shown in Fig.12(c). It is clear that layers with lower density (light contrast) and those with higher density (dark contrast) were formed one after another.

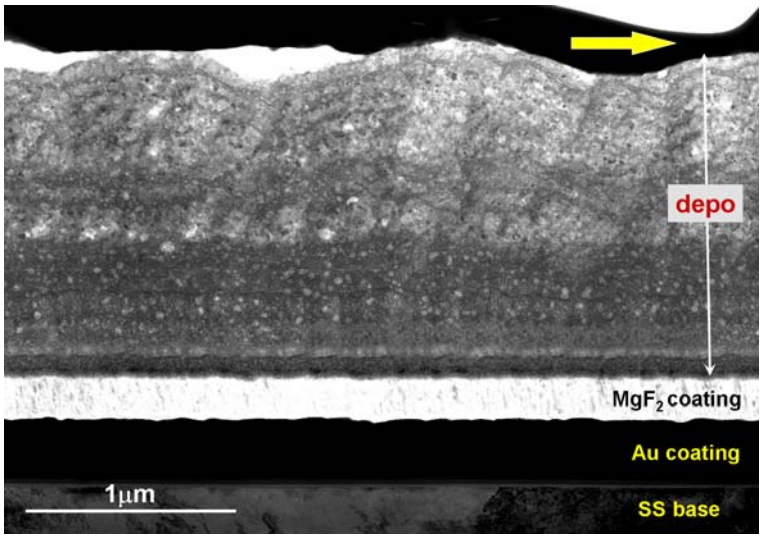

*Fig.10 Cross-sectional TEM image of the deposition at the point **e**.*

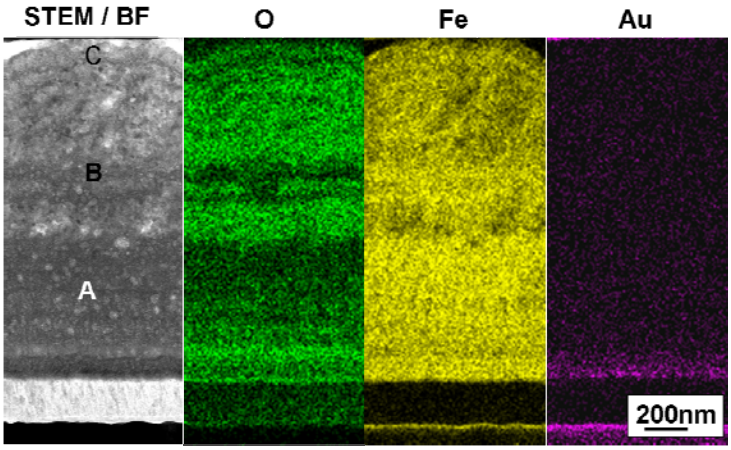

Fig.11 Two-dimensional distribution of O, Fe and Au in the deposition at the point e.

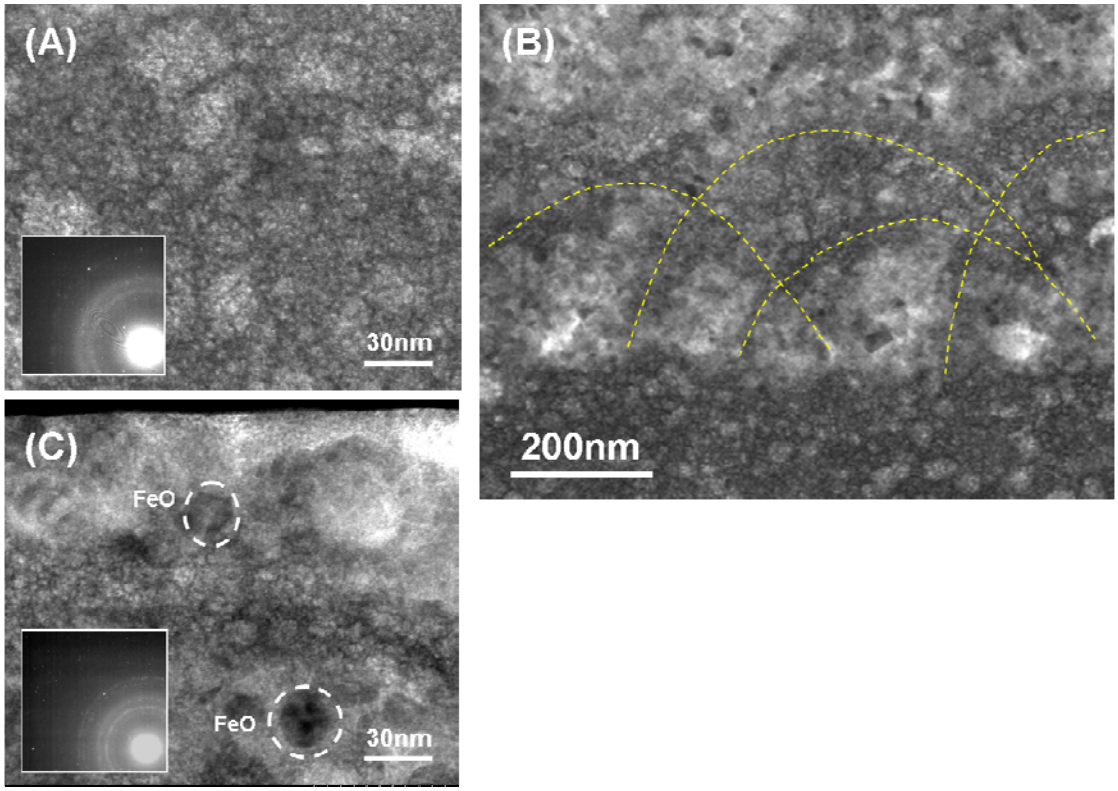

Fig 12 Magnified TEM micrographs at A, B and C.

4. Discussion

As described in Chapter 3, the mirror surfaces of the retro-reflectors placed on the protection wall of LHD suffered serious influence due to the plasma-wall interaction. The phenomena were complicate and different from place to place. At the area near the aperture, the plated gold layer of about 300nm-thick disappeared and the base made of stainless steel was also eroded. This result indicates that the reflector suffer serious sputtering erosion by high energy particles such as high energy charge exchange neutrals under main plasma discharges and plasma particles during DGC.

In case of He plasma discharges in LHD, typical energy contributing to material damage at the wall surface and its flux of the neutral He atoms were estimated to be about 1keV and $1x10^{19}$He/m^{2}s, respectively [10]. These data indicate that the sputtering rate of stainless steel placed on the protection wall is about $1x10^{-2}$nm/s. In case of H plasma discharges, neutral hydrogen with the similar energy and flux causes damage in materials placed on the wall surface [11]. Average sputtering rate under He-GDC is estimated to be $1x10^{-4}$nm/s. This value, however, depends on the distance from the electrode of the glow discharge. These estimations support the observed strong erosion around the aperture (point **a** in Fig. 2(a))

Around the cubic corner at the center, however, thick deposition composed of Fe, Cr, Ni, Au and O covered the original mirror surface. This result indicates that the impurities came from both vacuum vessel wall and reflector itself. Energetic particles of H and He which cause

sputtering erosion and the impurity atoms which cause deposition come to everywhere on the mirror surface, but the resulting phenomena is determined by delicate balance of the two factors, erosion dominant at point **a** and deposition dominant at points **c**, **d** and **e**. At point **b** erosion and deposition balanced each other out and the original gold surface could remain,

4.1 Pile-up of impurities at the cubic corner

The area near the cubic corner (points **c**, **d** and **e**), where the laser beam passed, was thickly covered by impurity deposition with very rough surface. Therefore formation mechanism of the rough surface is discussed in the following. On the mirror surface both high energy particles from the plasma and impurities come. The former sputter not only the mirror but also impurity atoms deposited on the surface. Some part of the sputtered atoms goes away from the reflector but some of them deposit again on the mirrors. As illustrated in Fig.13, deposited atoms are transported toward the cubic corner by the successive sputtering. At the area near the cubic corner deposited atoms have almost no way to get out form the reflector because each mirror is closely surrounded by the other two mirrors. Namely impurities deposited on the mirror surface pile-up at the narrow cubic corner part by the successive sputtering collision of the energetic particles from the plasma. We can say that impurity deposition is unavoidable for retro-reflectors if both impurities and high energy particles arrive on the mirror surfaces directly. High accumulation of sputtered impurities will occur not only in retro-reflectors but also roof reflectors and the parts where two or more surfaces meet together and form hollow structure, if they face plasma directly.

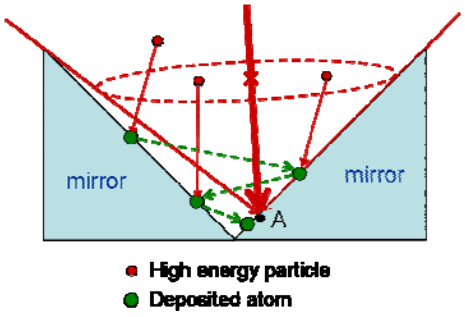

Fig. 13 Incident direction of impurities and high energy particles at point A, and inter-mirror movement of impurities by sputtering.

4.2 Formation mechanism of wavy surface

In case of ordinary vacuum deposition, surface of the deposited layer is very smooth but not as rough as that of the retro-mirror. Because it is expected that such surface roughening will cause the reduction of the optical reflectivity, understanding of the mechanism developing wave structure is very important. First of all, let us pay attention to the micrograph in Fig.7. Small hills and large projections incline toward the aperture. In the right-hand side of the large projection development of the small hills is slow. These results indicate that average injecting

direction of the impurities is not perpendicular to the mirror surface but inclined toward the aperture or the main plasma. If the injecting direction is inclined against the mirror surface as illustrated in Fig.14, wavy surface develop once the surface become uneven and development of the wavy structure is suppressed at the down stream area of the large projections due to the shadow effect of the projections. In case of the retro-reflectors average injection direction of impurities inclined against mirror surfaces, so once the surface become uneven the wave structure develop.

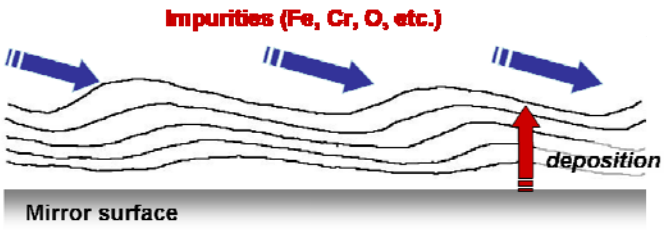

Fig. 14 Development of wavy surface by oblique injection of impurities.

4.3 Mechanisms of reflectivity reduction

Experimental results obtained by SEM and TEM observations indicate that possible mechanisms of the reflectivity reduction are followings.

(1) surface roughness due to formation of the hills
(2) formation of FeO
(3) formation of nano-scale dense bubbles

The result of Ni deposition effects shown in Fig. 9 strongly indicates that the serious reduction of the reflectivity at the visible wave length region can be explained by the formation of the dense hills of about 200-300nm-high. It is well known that the relative reflectivity of the uneven surface is given by the following equation [12].

$$\frac{R}{R_0} = \exp\left(-\left(\frac{4\pi\delta\cos\theta}{\lambda}\right)^2\right) \quad \cdots\cdots\cdots (1)$$

Here, R, R_0, δ, θ and λ are reflectivity, reflectivity of the flat surface, average roughness, reflection angle and wave length, respectively. In Fig. 15, measured reflectivity at the point **e** is compared with those estimated from equation (1) for several average roughness as a function of the wave length. The very low reflectivity at ultra-violet and visible wave length can be explained roughly by the surface roughness, but large reduction of the measured reflectivity at the longer wave length region can not be explained by the surface roughness alone.

In contrast, optical reflectivity of the FeO (wustite) is less than 20% even in the infrared region. The formation of FeO crystals is the major mechanism of the reflectivity reduction at infrared region. One should not that the co-deposition of metallic impurities and O is a very important factor deciding the reflectivity. According to the recent study on the irradiation

effects of He, formation of porous structure due to the dense fine bubbles also reduces the reflectivity even at infrared region [13]. It is likely that formation of bubbles is another reason for the reflectivity reduction.

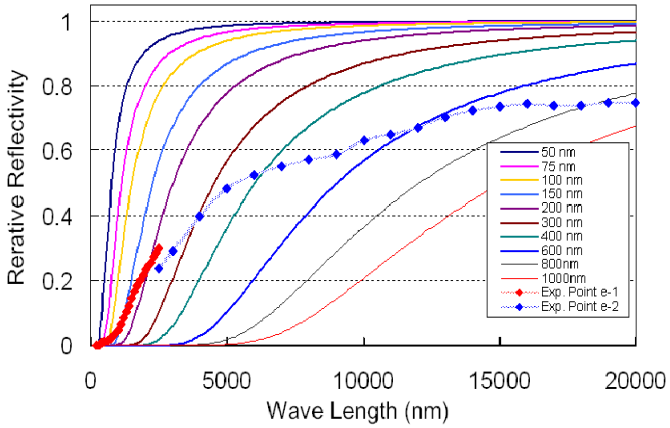

Fig.15 Wave length dependence of relative reflectivity, R/R_0, estimated form the equation (1) for various average roughness. Relative reflectivity (experimentally measured reflectivity/reflectivity of stainless steel) for the point e is also plotted for comparison.

4.4 Comparison with plasma discharge history

Roughly speaking, the deposition is composed of the layer with dark contrast and that with light contrast. The former is characterized by lower content of O, very fine FeO crystals and very dense bubbles which are formed typically under He irradiation but not by H irradiation. The latter is characterized by higher content of O, rather large FeO crystals and low bubble density. Formation of fine dense bubbles indicate strongly that the former layer with dark contrast is formed during He-DGC and the latter during main plasma discharge experiments.

By supposing the identification of the layers, it was tried to assign when each was formed by comparing the discharge history of the experimental cycle. Fig. 16 shows the layer structure of the deposition and the order of main discharge period and He-GDC period. They fit quite well. If the assignment is collect, it is likely that the formation of the blisters, which were the trigger of the wavy surface, occurred after the leakage of cooling water from NBI.

5. Summary

Optical reflectivity of the retro-reflector installed in LHD as the first mirror was seriously reduced by plasma wall interaction. In order to understand the mechanism of the reflectivity reduction, optical and material properties of the mirror surfaces have been examined extensively. Important results are the followings.

The surface of the retro-reflectors suffer very strong irradiation of high energy charge exchange neutrals of H and He during main plasma discharges and He ions under He-GDC. On the other hand impurity atoms ejected from the wall and the retro-reflector itself re-deposit on

the surface. The situation of the surface is determined by the balance of the two factors. At the periphery of the reflector sputtering erosion is dominant but at the cubic corner deposition is dominant. Impurities deposited on the surface are transported toward the cubic corner by the successive sputtering and pile-up around the corner. Deposition around the cubic corner reached 2μm-thick and its surface was covered by sub-micron hills. This rough surface reduces the reflectivity at the shot wave length region. Co-deposited Fe and O form fine FeO crystals. This is another reason for the reflectivity reduction especially at long wave length region. The deposition has clear layer structure depending on the condition of plasma discharge. The layer formed during He-GDC has very dense fine bubbles. This porous structure also reduces the reflectivity. The analysis of the layer structure indicates that leakage of water changed the surface properties and it leaded the formation of blisters of deposition. Once the blistering occurred the surface of the mirror became rough and resulted in the reflectivity reduction.

These experimental results are very useful for development of innovative retro-reflectors with long life time and also for understanding complicate plasma wall interactions in actual machines.

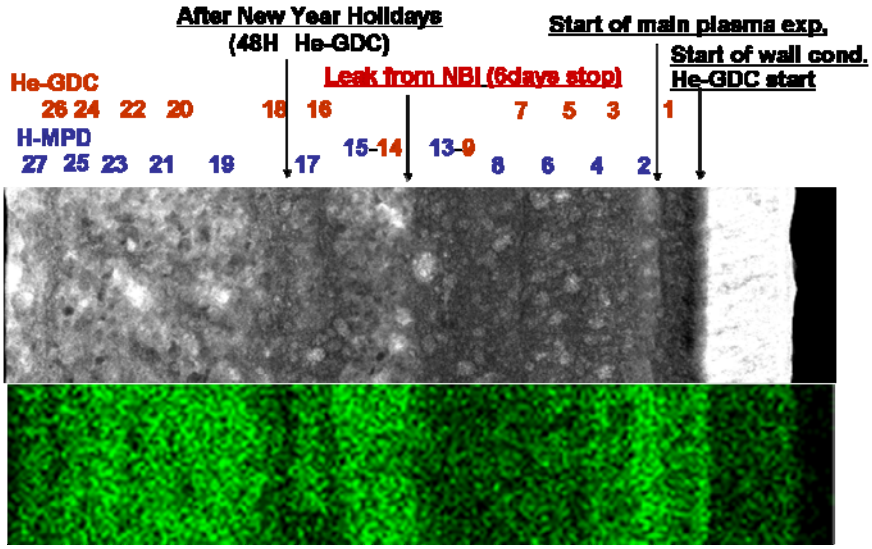

Fig. 16 Comparison of cross sectional microstructure of the deposition and with discharge history

Acknowledgments

This work is performed with the support and under the auspices of the NIFS Collaboration Research Program (NIFS08KCHH020). This work is partially supported by a Grant-in-aid for Scientific Research from Ministry of Education, Science and Culture of Japan.

References

[1] V.S. Voitsenya, A.F. Bardamid, V.T. Gritsyna *et. al.*, J. Nucl. Mater. 258-263(1998) 1919.

[2] V.S. Voitsenya, A.E. Costley, V. Bandourko *et. al.*, Rev. Sci. Instrum. 72 (2001) 475.

[3] V.S. Voitsenya, A.F. Bardamid, V.N. Bondarenko *et. al.*, J. Nucl. Mater. 290-293 (2001) 336.
[4] M. Balden, A.F. Bardamid, A.I. Belyacva *et al*. J. Nucl. Mater. 329-333 (2004), 1515
[5] V.S. Voitsenya, A.J.H. Donne, A.F. Bardamid *et. al.*, Rev. Sci. Instrum. **76**, 083502 (2005).
[6] L. Giudicotti, M. Brombin, S.L. Prunty *et. al.*, Rev. Sci. Instrum. 77 (2006) 123504.
[7] P. Wienhold, A. Litnovsky, V. Philipps et al. J. Nucl. Mater. 337-339 (2005) 1116
[8] M. Lipa, B. Schunke, Ch. Gil *et al*. Fusion Eng. And Design 81 221 (2006)
[9] T. Akiyama, K. Kawahata, N. Ashikawa, K. Tokitani, S. Okajima, K. Nakayama, N. Yoshida, A. Ebihara, K. Tokunaga, Y. Ohtawa, S. Tsuji-lio, to be published in Rev. Sci. Instrum
[10] M. Tokitani, M. Miyamoto, K. Tokunaga, T. Fujiwara, N. Yoshida, S. Masuzaki, N. Sahikawa, T. Morisaki, M. Shoji, A. Komori, LHD Experimental Group, S. Nagata, B. Tsuchiya, to be published in J. Nucl. Mater.
[11] M. Miyamoto et al., to be published.
[12] H.E. Bennet, J. Opt. Soc. Am. 53 (1961) 123.
[13] A. Ebihara, M. Tokitani, K. Tokunaga, T. Fujiwara, A. Sagara, N. Yoshida, J..Nucl. Mater. 363-365 (2007) 1195.